Available online at www.sciencedirect.com

SciVerse ScienceDirect

Geochimica et Cosmochimica Acta 84 (2012) 14–28

Geochimica et Cosmochimica Acta

www.elsevier.com/locate/gca

Stable iron isotope fractionation between aqueous Fe(II) and model Archean ocean Fe–Si coprecipitates and implications for iron isotope variations in the ancient rock record

Lingling Wu *, Elizabeth M. Percak-Dennett, Brian L. Beard, Eric E. Roden, Clark M. Johnson

Department of Geoscience, University of Wisconsin-Madison, 1215 West Dayton Street, Madison, WI 53706, United States
NASA Astrobiology Institute, 1215 West Dayton Street, Madison, WI 53706, United States

Received 7 April 2011; accepted in revised form 10 January 2012; available online 24 January 2012

Abstract

Iron isotope fractionation between aqueous Fe(II) ($Fe(II)_{aq}$) and two amorphous Fe(III) oxide–Si coprecipitates was investigated in an aqueous medium that simulated Archean marine conditions, including saturated amorphous silica, low sulfate, and zero dissolved oxygen. The equilibrium isotope fractionation (in $^{56}Fe/^{54}Fe$) between $Fe(II)_{aq}$ and Fe(III)-Si coprecipitates at circum-neutral pH, as inferred by the three-isotope method, was -3.51 ± 0.20 $(2\sigma)‰$ and -3.99 ± 0.17 $(2\sigma)‰$ for coprecipitates that had Fe:Si molar ratios of 1:2 and 1:3, respectively. These results, when combined with earlier work, indicate that the equilibrium isotope fractionation factor between $Fe(II)_{aq}$ and Fe(III)–Si coprecipitates changes as a function of Fe:Si ratio of the solid. Isotopic fractionation was least negative when Fe:Si = 1:1 and most negative when Fe:Si = 1:3. This change corresponds with changes in the local structure of iron, as revealed by prior spectroscopic studies. The kinetics of isotopic exchange was controlled by movement of Fe(II) and Si, where sorption of Fe(II) from aqueous to solid phase facilitated atom exchange, but sorption of Si hindered isotopic exchange through blockage of reactive surface sites. Although Fe(II)–Fe(III) isotopic exchange rates were a function of solid and solution compositions in the current study, in all cases they were much higher than that determined in previous studies of aqueous Fe(III) and ferrihydrite interaction, highlighting the importance of electron exchange in promoting Fe atom exchange. When compared to analogous microbial reduction experiments of overlapping Fe(II) to Fe(III) ratios, isotopic exchange rates were faster in the biological experiments, likely due to promotion of atom exchange by the solid-phase Fe(II) produced in the biological experiments. These results provide constraints for interpreting the relatively large range of Fe isotope compositions in Precambrian marine sedimentary rocks, and highlight important differences between modern and ancient marine environments due to the absence or presence of dissolved silica. Evidence can be found in the Fe isotope compositions of the ancient rock record for both abiologic and biologic processes, distinction of which becomes apparent when sedimentological and diagenetic processes are fully explored, as well as Fe mass balance.

* Corresponding author at: Department of Geoscience, University of Wisconsin-Madison, 1215 West Dayton Street, Madison, WI 53706, United States. Tel.: +1 608 890 0929.
E-mail address: lwu@geology.wisc.edu (L. Wu).

0016-7037/$ - see front matter © 2012 Elsevier Ltd. All rights reserved.
doi:10.1016/j.gca.2012.01.007

1. INTRODUCTION

Precambrian marine sedimentary rocks that formed at low temperatures, including shales, carbonates, and banded iron formations, contain the largest inventories of isotopically fractionated Fe in the Earth's crust (e.g., Anbar and Rouxel, 2007; Johnson et al., 2008b). Redox processes are known to produce large Fe isotope fractionations at low temperatures in modern marine and fresh-water environments (e.g., Bergquist and Boyle, 2006; Fehr et al., 2008; Teutsch et al., 2009; Severmann et al., 2010), which suggests that redox changes, driven by biology or not, were likely responsible for Fe isotope fractionation in Precambrian marine environments. In addition, partial utilization of aqueous Fe(II) ($Fe(II)_{aq}$) during abiotic pyrite formation has been recently suggested to be responsible for the negative $\delta^{56}Fe$ excursion in the ancient rock record (Guilbaud et al., 2011).

Precambrian marine systems had relatively high dissolved Fe(II) and silica, and the interaction of these species and iron oxyhydroxides comprised the ancient Fe cycle. Today, amorphous Fe(III) oxides ($Fe(III)_{am}$) is one of the most important components of the Fe cycle in sedimentary environments (Cornell and Schwertmann, 2003). Silica may prevent phase transformation of $Fe(III)_{am}$ in the presence of Fe(II), either in the dissolved form or synthesized together with $Fe(III)_{am}$ (Wu et al., 2011). Equilibrium Fe(II)–$Fe(III)_{am}$ $^{56}Fe/^{54}Fe$ fractionation factors of -3.17 ± 0.08 (2σ)‰ and -2.58 ± 0.14 (2σ)‰ have been obtained for $Fe(III)_{am}$ plus silica in solution and Fe(III)–Si coprecipitate (referred to hereafter as Fe–Si CP), respectively (Wu et al., 2011), indicating an important control by silica. The equilibrium Fe(II)–$Fe(III)_{am}$ $^{56}Fe/^{54}Fe$ fractionation factor in the absence of silica in solution has been inferred to be ~ -3.2‰ (Wu et al., 2011).

Microbial dissimilatory iron reduction (DIR) has been proposed to play a significant role in producing Fe isotope fractionations recorded in both modern and ancient marine environments (e.g., Beard et al., 2003; Staubwasser et al., 2006; Johnson et al., 2008a; Tangalos et al., 2010). Coupled electron and atom exchange has been shown to be the mechanism for Fe isotope fractionation during microbial dissimilatory iron reduction (Crosby et al., 2007; Wu et al., 2009; Percak-Dennett et al., 2011), as well as abiological interaction between $Fe(II)_{aq}$ and various Fe(III) oxides (Beard et al., 2010; Wu et al., 2011). The importance of electron transfer in promoting Fe atom exchange is clearly illustrated by the much greater extent of exchange between $Fe(II)_{aq}$ and all $Fe(III)_{am}$ phases (Wu et al., 2011), as compared to that documented for interaction of aqueous Fe(III) and pure $Fe(III)_{am}$, where redox-driven electron exchange does not occur (Poulson et al., 2005). The majority of previous experimental studies of Fe isotope fractionations produced during DIR have used conditions analogous to freshwater systems (Icopini et al., 2004; Crosby et al., 2005, 2007; Johnson et al., 2005), although one study has looked at the effects of pH and dissolved silica on DIR-driven Fe isotope fractionation (Wu et al., 2009). A recent study investigated Fe isotope fractionation produced by DIR under conditions that simulated key aspects of Archean marine conditions, through use of an artificial seawater medium that contained dissolved silica and an amorphous Fe(III) oxide–silica coprecipitate designed to mimic the electron acceptors that likely existed in Archean ocean sediments (Percak-Dennett et al., 2011). Rapid and near-complete isotopic exchange was found among all Fe(II) and Fe(III) components in the DIR system (Percak-Dennett et al., 2011), in contrast to previous work on goethite and hematite (e.g., Crosby et al., 2005, 2007; Wu et al., 2009), where exchange was limited to the outer few atom layers of the substrate. Microbial reduction of Fe–Si CP produced large quantities of aqueous, sorbed, and solid-phase Fe(II) that had low-$\delta^{56}Fe$ values, providing strong support for DIR as an efficient means for producing the Fe isotope variations observed in the ancient rock record (Percak-Dennett et al., 2011).

In this study, the Fe isotope fractionation between $Fe(II)_{aq}$ and Fe–Si CPs was determined under simulated Archean seawater conditions. A comparison of the experimental conditions in the current and previous studies (Percak-Dennett et al., 2011; Wu et al., 2011) is shown in Table 1. The aim of the current study was to investigate Fe isotope exchange and fractionation in an abiological system analogous to the DIR system studied by Percak-Dennett et al. (2011). Moreover, we sought to obtain demonstrably equilibrium isotope fractionation factors, which are key to interpreting biological, as well as abiological systems. To achieve this, the three-isotope method was employed to determine the equilibrium Fe isotope fractionation factor that would be achieved during complete isotope exchange (e.g., Matsuhisa et al., 1978; Beard et al., 2010), an approach not possible in biological systems where the proportions of Fe(II) and Fe(III) change due to enzymatic processes. The three-isotope method involved isotope exchange between an isotopically normal component and an isotopically enriched component (Fig. 1). The equilibrium fractionation factor can be inferred by extrapolating partially exchanged samples to the intercept with the secondary mass–fractionation line, which is parallel to the primary mass–fractionation line and passes through the isotopic composition of the system, as dictated by mass balance. This method has been applied to oxygen, iron, chromium, and magnesium isotope systems (e.g., Matsuhisa et al., 1978; Shahar et al., 2008; Beard et al., 2010; Zink et al., 2010; Li et al., 2011). In addition, we explored the effects of Fe:Si molar ratio of the oxyhydroxide on equilibrium Fe isotope fractionation factors.

2. METHODS

2.1. Experimental design and materials

Iron isotope fractionations were investigated during interaction between $Fe(II)_{aq}$ and two different Fe–Si CP phases in Archean Artificial Seawater (AAS) medium (Percak-Dennett et al., 2011), where Fe–Si CP nanoparticles were aged with $Fe(II)_{aq}$. The AAS was based on the artificial seawater recipe of Kester et al. (1967), modified through reduction of Na_2SO_4 to a concentration ($\approx$200 μM), comparable to values suggested for Archean seawater (Habicht

Table 1
Experimental conditions and equilibrium Fe isotope fractionation factors between $Fe(II)_{aq}$ and different amorphous Fe(III) oxides at 20 °C.

	System	Solid synthesis	Fe:Si of solid	Aqueous solution	$\Delta^{56}Fe$ (‰)	Reference
$Fe(II)_{aq}$–$Fe(III)_{am}$[a]	Abiological	$Fe(III)_{aq}$ hydrolysis	No Si	10 mM PIPES[b]+2.14 mM Si (pH = ~7)	−3.17 ± 0.08	Wu et al. (2011)
$Fe(II)_{aq}$–Fe–Si CP[c]	Abiological	$Fe(III)_{aq}$ hydrolysis in Si solution	1:1	10 mM PIPES[b] (pH = ~7)	−2.58 ± 0.14	Wu et al. (2011)
$Fe(II)_{aq}$–Fe–Si CP1	Abiological	$Fe(II)_{aq}$ oxidation	1:2	AAS (pH = 6.7)[d]	−3.51 ± 0.20	This study
$Fe(II)_{aq}$–Fe–Si CP2	Abiological	$Fe(II)_{aq}$ oxidation	1:3	AAS (pH = 6.7)[d]	−3.99 ± 0.17	This study
$Fe(II)_{aq}$–Fe–Si CP1	DIR[e]	$Fe(II)_{aq}$ oxidation	1:2	AAS (pH = 6.5)[d]	−2.82 ± 0.19	Percak-Dennett et al. (2011)

[a] Silica was present in solution (2.1 mM) to prevent phase transformation of $Fe(III)_{am}$.
[b] PIPES denotes 1, 4-piperazine-N, N′-bis-2-ethanesulfonic acid, sesquisodium salt buffer.
[c] Fe–Si CP produced by hydrolysis of $FeCl_3 \cdot 6H_2O$ in the presence of Si, and reacted with $Fe(II)_{aq}$ in Si-free solution.
[d] Detailed composition for Artificial Archean Seawater (AAS), which includes 2.14 mM Si, 0.1 mM phosphate, and very low sulfate, and additional ions to simulate seawater, can be found in Percak-Dennett et al. (2011).
[e] The isotope fractionation factor determined in biological system may not represent equilibrium fractionation but rather leveling off of isotopic exchange at about ~80% (assuming the same equilibrium fractionation as in the abiological system for Fe–Si CP1) due to blockage of reactive surface sites on the solid by adsorbed Si.

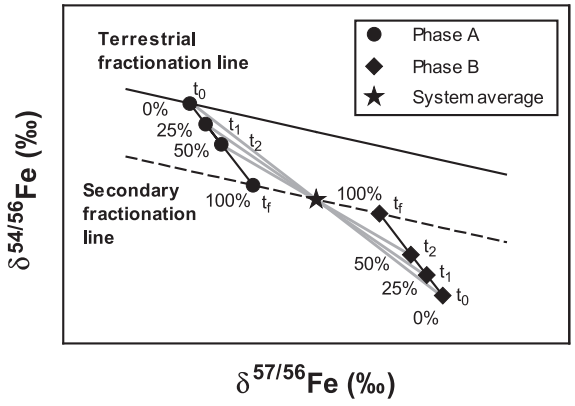

Fig. 1. Schematic diagram of the three-isotope method as applied to a two-component Fe system. Mass-dependent fractionation of Fe isotopes defines a terrestrial fractionation line that has a slope of −2.105 for $\delta^{54/56}Fe$ vs. $\delta^{57}/^{56}Fe$. Phase A initially lies on the terrestrial fractionation line and phase B is initially enriched in ^{57}Fe (phase A and phase B do not necessarily have the same $\delta^{54/56}Fe$ values). As isotopic exchange proceeds between the two phases, their isotopic compositions will evolve towards 100% exchange. The final isotopic compositions of A and B at complete exchange lie on a secondary fractionation line, which is parallel to the terrestrial line and passes through the isotopic composition of the system, as dictated by mass balance. Extrapolation of partially exchanged samples to the intercept with the secondary fractionation line determines the isotopic composition of phases A and B at complete exchange; if isotopic exchange occurs under equilibrium conditions, this will reflect the equilibrium isotope fractionation factor.

et al., 2002), and addition of 0.608 g L^{-1} $Na_2SiO_3 \cdot 9H_2O$ to account for the high dissolved silica content of the Precambrian oceans (e.g., Maliva et al., 2005; Konhauser et al., 2007). Two sets of isotope exchange experiments were conducted: (1) ^{57}Fe-spiked Fe(II) + "normal" Fe–Si coprecipitate 1 (Fe–Si CP1); (2) "normal" Fe(II) + ^{57}Fe-spiked Fe–Si coprecipitate 2 (Fe–Si CP2). Duplicate reactors (a and b) were set up for each set of experiments.

A stock solution of Fe(II) that had "normal" isotopic composition was prepared by dissolving $FeCl_2 \cdot 4H_2O$ in 0.5 M HCl in an anaerobic chamber (Coy Products, Grass Lake, MI). All the solutions were bubbled with O_2-free N_2 before introduction to the anaerobic chamber. A ^{57}Fe-enriched Fe(II) stock solution was prepared by first dissolving pure ^{57}Fe metal (Chemgas) in 1.4 M HCl (final molarity after reaction was 0.5 M), followed by mixing with isotopically "normal" Fe(II) solution. All preparations were carried out in the anaerobic chamber, and the stock solutions were confirmed to be purely ferrous by chemical analysis. An isotopically "normal" Fe–Si CP was prepared following the protocol developed by Percak-Dennett et al. (2011). A ^{57}Fe-enriched Fe–Si CP was synthesized by mixing equal molarity of $NaHCO_3$ and Na_2SiO_3 with ^{57}Fe-enriched $FeCl_2$, and the mixture was allowed to oxidize in open exchange with the atmosphere for 8 days. The proportion of Fe(III) in the final solid was 97% of total Fe. The solid was centrifuged and rinsed four times with H_2O to remove excess salt. Analyses using X-Ray Diffraction (XRD) and Transmission Electron Microscopy (TEM) showed that both ^{57}Fe-enriched and isotopically "normal" Fe–Si CP remained amorphous over the course of the experiments (Electronic Annex Figs. EA1 and EA2).

Experiments were carried out in separate 10 mL serum glass bottles with 10 mL anaerobic (N_2 & CO_2-bubbled) AAS media that contained 2 mmol L^{-1} of Fe–Si CP. The experiments were initiated by addition of 2 mM $FeCl_2$ from an anaerobic stock solution. Repeated tests showed that the pH of the solutions was ~6.7 after adding $FeCl_2$. Experiments were conducted for 28 days. All sampling was carried out in the anaerobic chamber. The maintenance of anaerobic conditions was confirmed by complete recovery of Fe(II) (see Section 2.2.).

2.2. Fe phase separation and chemical analysis

Bottles that contained 10 mL aliquots of the reaction slurries were centrifuged to remove the aqueous fraction at 0.5 h, and 2, 3, 5, 7, 10, 20, and 28 days after initiation

of the experiments (Fig. 2). The remaining solids were extracted for 15 min using 5 mM HCl, which removed the easily extractable, presumably "sorbed" Fe(II), without dissolving any underlying Fe(III); this was confirmed by Fe(II) and total Fe measurements, which indicated Fe(III) levels were not detectable (Electronic Annex Table EA2). Fe(II) was measured directly using *Ferrozine* (Stookey, 1970), total Fe was measured using *Ferrozine* after reducing Fe(III) with hydroxylamine hydrochloride, and Fe(III) was determined by difference. The remaining solids were dissolved using 0.5 M HCl. A white gel that contained pure silica remained after the 0.5 M HCl dissolution step, and this gel could only be dissolved using 1 M NaOH. Silica concentrations for different fractions were analyzed using a colorimetric method (Clesceri et al., 1989). The Fe:Si ratios were 1:2 and 1:3 for Fe–Si CP1 and Fe–Si CP2, respectively, as determined by complete digestion of the starting materials using HCl and NaOH.

Complete recovery of Fe(II) ($97 \pm 9\%$) and Fe(III) ($101 \pm 10\%$) was achieved by combining Fe(II) and Fe(III) in all three fractions (aqueous, acid extract, and residue), where the uncertainties reflect weight and volume errors. Fe(II) in the 0.5 M HCl extraction was measured using NH_4F to mask the influence of Fe(III) on the absorption spectra (Krishnamurti and Huang, 1990). All samples were passed through 0.2 μm filters, and the aqueous fraction and acid extract were acidified with HCl.

2.3. Fe isotope measurements and nomenclature

All $Fe(II)_{aq}$ and HCl extract solutions were purified using anion-exchange chromatography, followed by Fe isotope analysis using a MC-ICP-MS, as previously described (Beard et al., 2003). A fast-washout cyclonic spray chamber, cooled to 5 °C with a 100 μL min^{-1} self aspirating nebulizer, was used for sample introduction to facilitate washout between samples that may have markedly different Fe isotope compositions. In addition, the potential difference between extraction and skimmer cones was decreased to avoid memory effects (Beard et al., 2010). Data are reported as $^{56}Fe/^{54}Fe$ ratios relative to the average of igneous rocks, in standard δ notation: $\delta^{56}Fe = [(^{56}Fe/^{54}Fe_{sample})/(^{56}Fe/^{54}Fe_{std}) - 1] \times 10^3$, where $^{56}Fe/^{54}Fe_{std}$ is the average of igneous rocks. Values for $\delta^{57/56}Fe$ may be defined in an analogous manner using the $^{57}Fe/^{56}Fe$ ratio. Measured external precision for $\delta^{56}Fe$ is 0.10‰ (2σ) and the precision for $\delta^{57}/^{56}Fe$ values is slightly poorer at 0.14‰ (2σ), as determined by replicate analysis of 33 samples, including 10 samples separately processed through anion-exchange chromatography (out of 132 samples, reported in Tables EA1, EA3, & EA6 in Electronic Annex). The measured isotope composition of the IRMM-014 standard is $\delta^{56}Fe$ of -0.09 ± 0.06‰ and $\delta^{57/56}Fe$ of -0.02 ± 0.10‰ (2σ, $n = 7$).

The Fe isotope compositions of the starting materials were assessed for their isotopic homogeneity (Electronic Annex Table EA1). Partial dissolution tests using HCl of different strengths (10, 20, 50, or 100 mM) for 5 min showed that for the isotopically "normal" Fe–Si CP1, the HCl extractable component had a slightly higher $\delta^{56}Fe$ value than the remaining solid. For the ^{57}Fe-enriched Fe–Si CP2, the difference between the HCl extractable component and the remaining solid was much smaller, with the exception of the 10 mM HCl extraction. However, the maximum range in $\delta^{56}Fe$ values for all partial extractions was fairly small (0.53‰) compared with the much larger range observed during Fe(II) and Fe–Si CP interactions. Given the relative ease with which isotopic exchange occurs between $Fe(II)_{aq}$ and the Fe–Si CP, as discussed below, the most likely explanation for the small range in $\delta^{56}Fe$ values measured in the partial extractions is re-equilibration between residual Fe–Si CP and dissolved Fe during partial dissolution. We therefore conclude that the Fe–Si CP likely had a homogeneous Fe isotope composition, certainly sufficient such that the results are not affected.

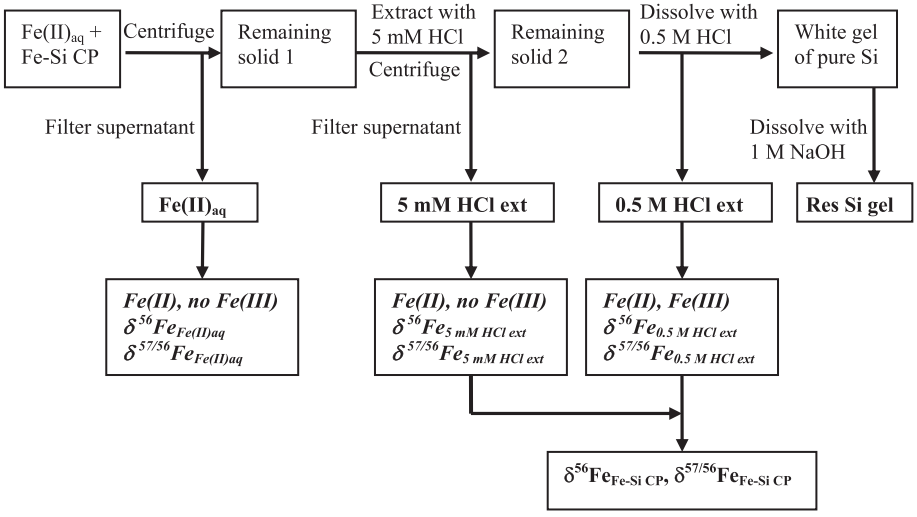

Fig. 2. Schematic flow chart showing extraction methods used in the experiments. Measured Fe concentrations and isotopic compositions are shown in italics. The isotopic composition for the Fe–Si CP was calculated by subtracting the Fe(II) component and assuming the Fe(II) in 0.5 M HCl extract has the same isotopic composition as the Fe(II) in 5 mM HCl extract.

Stable Fe isotope fractionation between two components A and B are described as $\alpha^{56}_{A-B} = (^{56}Fe/^{54}Fe_A)/(^{56}Fe/^{54}Fe_B)$, following standard practice. Under equilibrium conditions, α^{56}_{A-B} reflects fundamental differences in the thermodynamic properties of components A and B (Schauble, 2004). To a very good approximation, α^{56}_{A-B} may be related to differences in the $\delta^{56}Fe$ values through the relation: $\Delta^{56}Fe_{A-B} = \delta^{56}Fe_A - \delta^{56}Fe_B \approx 10^3 \ln \alpha^{56}_{A-B}$.

2.4. Calculation of fraction of isotopic exchange *F*

The fraction of Fe isotope exchange at any time (F_t) can be described by the following equation $F_t = (\delta_t - \delta_i)/(\delta_e - \delta_i)$, where δ_t is the isotope composition at time t, δ_i is the isotope composition of the starting material, and δ_e is the equilibrium isotope composition; for experiments using enriched tracers, δ_e may be estimated based on the mass balance of each reactor, as calculated by the sum of the isotope composition of each component, multiplied by the mass proportion of each component. In our experiments, the mass balance of the system may be constrained within a 2% error (one standard deviation divided by the mean, see Table EA5). Calculation of F using either $Fe(II)_{aq}$ or residual Fe–Si CP agreed within 8% on average, as should be the case in a two-component system. $\delta^{57/56}Fe$ values were used to calculate *F* because a ^{57}Fe-enriched tracer was used, and this minimizes (but does not completely eliminate) the effects of mass-dependent fractionation in estimating δ_e.

3. RESULTS

3.1. Kinetics of isotope exchange between aqueous Fe(II) and Fe–Si coprecipitates

Fig. 2 provides a flow diagram which explains how different Fe pools were separated by sequential extraction methods. Although great care was taken to completely separate different components, it is possible that a small amount of residual aqueous Fe(II) was recovered in the 5 mM HCl extraction. The 5 mM HCl extraction did not dissolve any Fe–Si CP, as demonstrated by zero Fe(III) in the extract (Table EA2). A small amount of Fe(II) was recovered in the 0.5 M HCl extract, however, the exact nature of this Fe(II) was not clear. It is possible that this Fe(II) reflected carry-over of Fe(II) that was not recovered in the 5 mM HCl extraction. This was, however, taken into account when calculating the isotopic composition for the solid by assuming that Fe(II) in the 0.5 M HCl extract has the same isotopic composition as that measured in the 5 mM HCl extract.

Aqueous Fe(II) and Fe recovered in the 0.5 M HCl extract dominated Fe mass balance in the experiments, whereas Fe in the 5 mM HCl extract accounted for only a small portion (<13%) of total Fe (Fig. 3; see also Electronic Annex Fig. EA3 and Table EA2). The $Fe(II)_{aq}$ concentration decreased with time, accompanied by an increase in the Fe(II) in the HCl-extractions, reflecting net transfer of Fe(II) from aqueous to solid phase (Fig. 3, Fig. EA3, Table EA2). The behavior of Si was similar to that of Fe: aqueous Si decreased with time, whereas Si in the acid extract slightly increased. Most of the solid-associated Si was recovered as a residual Si gel that was not soluble in 0.5 M HCl (Fig. 3). It is likely that this Si was amorphous silica that precipitated as the Fe–Si CP dissolved in acid.

For all experiments, the initial time point (sampled 30 min after mixing) showed a significant change in isotopic composition (Fig. 4; see also Tables EA1 and EA3),, reflecting rapid initial isotopic exchange followed by slower exchange. The relation between the fraction of exchange and time cannot be described by a simple 2nd order reaction (Fig. 3e and f); this is in contrast, for example, to previous studies on isotopic exchange between $Fe(II)_{aq}$ and $Fe(III)_{aq}$ at acidic pH (Johnson et al., 2002; Welch et al., 2003).

3.2. Measured isotope fractionation between Fe(II) and Fe–Si coprecipitates

Extrapolation of the mass-dependent Fe isotope fractionations to complete exchange produced an average $^{56}Fe/^{54}Fe$ fractionation of -3.51 ± 0.20 (2σ)‰ between $Fe(II)_{aq}$ and Fe–Si CP1, and -3.99 ± 0.17 (2σ)‰ between $Fe(II)_{aq}$ and Fe–Si CP2 (Fig. 5, Table 2). These two fractionation factors are different from those determined previously for $Fe(II)_{aq}$ and pure $Fe(III)_{am}$ in 2.1 mM aqueous Si solution, and $Fe(II)_{aq}$ and Fe–Si CP in Si-free solution (Table 1). The measured $^{56}Fe/^{54}Fe$ fractionation factor between $Fe(II)_{aq}$ and easily-extractable (15 min leach in 5 mM HCl), presumably surface-associated (i.e., sorbed) solid-phase Fe(II) changed significantly from +0.96‰ upon mixing (initial time point) to −0.21‰ after 2 days (2nd time point), and from +1.16‰ upon mixing to −0.07‰ after 2 days for Fe–Si CP1 and Fe–Si CP2 experiments, respectively (Figs. 4 and EA4, Table EA3). The distinct initial isotope composition for the acid extract implies that a new component was formed on the surface of the solid, and that this component had a $\delta^{56}Fe$ value that is more negative than $Fe(II)_{aq}$, possibly as a result of kinetic fractionation. This new surface component has a $\delta^{57/56}Fe$ value closer to that of the solid, but this is unlikely to reflect contamination from the solid during separation, because such an explanation would produce very high levels of Fe(III) that was not detected. The $\delta^{57/56}Fe$ value of the new surface component moved towards that of the $Fe(II)_{aq}$ with time (Fig. 4), indicating isotopic exchange. The final $^{56}Fe/^{54}Fe$ fractionation factor between $Fe(II)_{aq}$ and Fe in the 5 mM HCl extract reached −1.11‰ and −0.68‰ after 28 days for Fe–Si CP1 and Fe–Si CP2, respectively. These values were similar to the equilibrium fractionation between $Fe(II)_{aq}$ and sorbed Fe(II) of ~−0.8‰ observed in previous experiments with pure $Fe(III)_{am}$ and Fe–Si CP (Wu et al., 2011).

4. DISCUSSION

Below we review the basis for inferring equilibrium fractionation factors, followed by a discussion of the effects of Fe and Si on the fractionation factors in terms of likely structural changes. Next we review the isotopic exchange

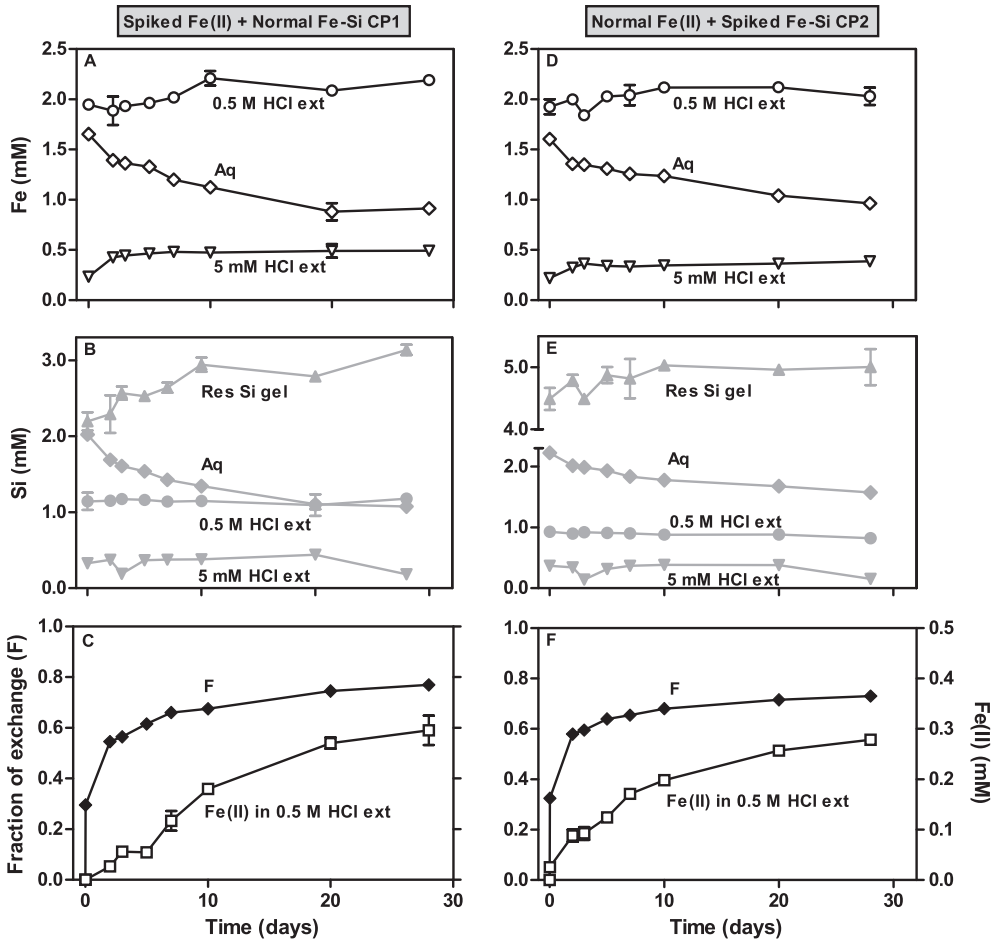

Fig. 3. Temporal variation of Fe (A & D) and Si (B & E) concentrations in the aqueous phase, and the 5 mM and 0.5 M HCl extracts of the Fe–Si CP. Panels C & F show fraction of exchange (left axes) and Fe(II) concentration in the 0.5 M HCl extract of the Fe–Si CP (right axes). Error bars indicate range of duplicate reactors. Fe–Si CP1 had an Fe:Si ratio of 1:2 and Fe–Si CP2 has an Fe:Si ratio of 1:3.

kinetics observed in the current study, and compare these results to those of previous biological experiments, which bear on the likelihood that abiologic and biologic systems may attain Fe isotope equilibrium. Finally, we conclude with a discussion of the implications of our findings for interpreting Fe isotope data from natural systems, both modern and ancient.

4.1. Equilibrium nature of measured Fe isotope fractionation factors

The three-isotope method allows robust constraints to be made on the isotopic fractionation that occurs at 100% exchange, which reflects conditions of isotopic equilibrium if the mechanism of exchange does not impart kinetic effects. It is possible, however, that precipitation/dissolution reactions may impose a kinetic isotope fractionation even at 100% isotopic exchange (e.g., Li et al., 2011). When recystallization process such as "Ostwald ripening" occurs, growth of larger crystals is achieved through dissolution of smaller crystals (e.g., Stoffregen et al., 1994). The dissolution reaction is not expected to impose an isotopic fractionation because the reaction is unidirectional and complete. Instead, any kinetic fractionation would most likely occur by the precipitation reaction when mineral growth occurs. In the current study, XRD and TEM work confirmed that the solids remained amorphous throughout all of the experiments. TEM images showed no evidence of localized Fe- or Si-rich areas, indicating that the material was homogeneous at the nm scale. This observation agrees with previous findings that Fe and Si do not polymerize separately during the hydrolysis method used to produce CP1 and CP2, but rather form phases in which Fe and Si are intimately associated (Doelsch et al., 2003). Experimental work using FTIR (Fourier Transform Infrared Spectroscopy) and ^{29}Si NMR (Nuclear Magnetic Resonance) (Doelsch et al., 2001) suggests that Si–O–Fe bonds likely existed in all of the precipitates used in this study where Fe:Si ratios lie between 1:1 and 1:3 at pH 7. We conclude that the homogeneous nature of the solid, and the highly labile nature of the Fe–Si CP, makes it unlikely that kinetic isotope effects occurred in our experiments. In addition, if a kinetic fractionation occurred during precipitation via transport to the mineral–solution interface, the light isotopes would likely partition into the newly formed solid, which is opposite to what was measured in our experiments (Fig. 4).

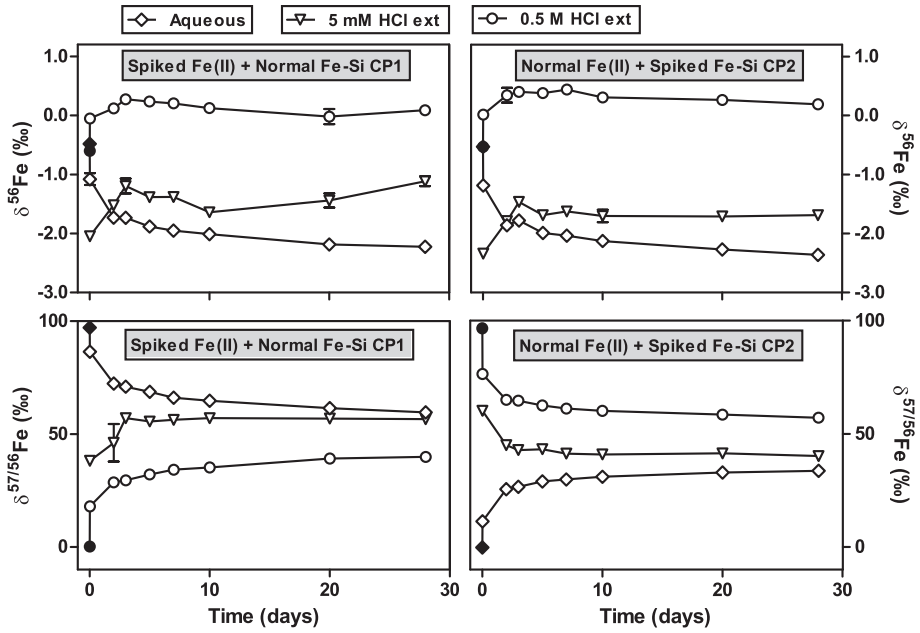

Fig. 4. Temporal variation of Fe isotope compositions for aqueous Fe(II) and the 5 mM and 0.5 M HCl extracts of Fe–Si CP. Error bars indicate range of duplicate reactors. Filled symbols represent isotopic composition for the starting materials.

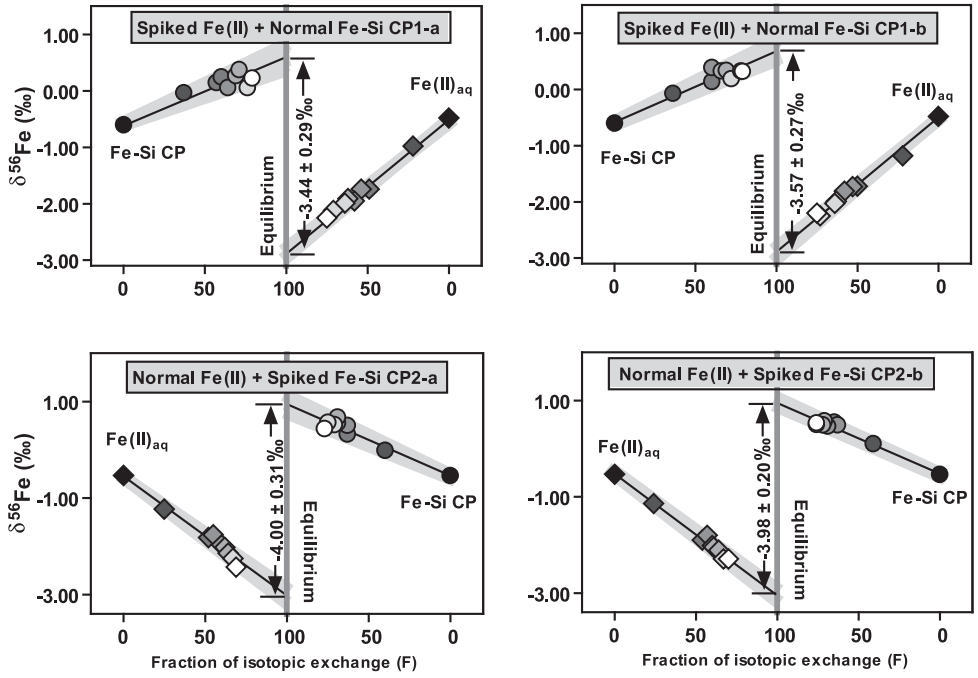

Fig. 5. Plot of isotope composition versus fraction of isotopic exchange (F). Isotopic compositions at complete exchange are obtained by extrapolating to 100% isotopic exchange. Isotopic compositions for Fe–Si CPs were calculated by subtracting the Fe(II) component in the 0.5 M HCl extract. Symbols are shaded where the darkest symbols represent starting materials and the lightest symbols represent final time points. Errors represent 2 standard deviation.

Operationally, Fe(II) in the 0.5 M HCl extract of the Fe–Si CP increased with time (Fig. 3). The fact that this Fe(II) is not removable by 5 mM HCl extraction, but can only be recovered by 0.5 M HCl, suggests that it was bound more strongly to the solid than the easily removable "sorbed" Fe(II). The observation of increasing Fe(II) in the solid is common in systems involving interactions between aqueous Fe(II) and Fe(III) oxyhydroxides (e.g., Williams and Scherer, 2004; Beard et al., 2010; Wu et al., 2010). This should not be interpreted as reflecting changes in the

Table 2
Extrapolated Fe isotope composition of $Fe(II)_{aq}$ and Fe–Si CP at equilibrium.

Experiment	$Fe(II)_{aq}$ $\delta^{56}Fe$ (‰)	Fe–Si CP $\delta^{56}Fe$ (‰)	$\Delta^{56}Fe$ (‰)$_{Fe(II)aq–(Fe–Si\ CP)}$	2σ
Spiked Fe(II) + Normal Fe–Si CP1a	−2.86	0.58	−3.44	0.29
Spiked Fe(II) + Normal Fe–Si CP1b	−2.88	0.69	−3.57	0.27
Average for duplicate experiments			−3.51	0.20
Normal Fe(II) + Spiked Fe–Si CP2a	−3.04	0.96	−4.00	0.31
Normal Fe(II) + Spiked Fe–Si CP2b	−3.02	0.96	−3.98	0.20
Average for duplicate experiments			−3.99	0.17

nature of the solid because XRD and TEM analysis provided no evidence for formation of new mineral phases. In addition, we were able to completely recover all the Fe(III) that was initially added to the system, which rules out possible formation of small amounts of more crystalline Fe(III) oxide phases. Therefore, we infer that the extrapolated isotope fractionations at 100% exchange are representative of equilibrium fractionation factors for $Fe(II)_{aq}$ and $Fe(III)_{am}$ in the Fe–Si CPs.

4.2. Effects of Fe:Si molar ratio on equilibrium Fe isotope fractionation factors

The inferred equilibrium $^{56}Fe/^{54}Fe$ fractionation between $Fe(II)_{aq}$ and the $Fe(III)_{am}$ component of various solids ($\Delta^{56}Fe_{Fe(II)aq–Fe(III)am}$) changed as a function of the Fe:Si molar ratio of the solid (whose isotopic composition was determined by 0.5 M HCl dissolution) (Fig. 6). The $\Delta^{56}Fe_{Fe(II)aq–Fe(III)am}$ fractionation was −3.17‰ with no Si (Wu et al., 2011), −2.58‰ with 1:1 Fe:Si (Wu et al., 2011), −3.51‰ with 1:2 Fe:Si (this study), and −3.99‰ with 1:3 Fe:Si (this study). The speciation change induced by different medium compositions (Table 1) is unlikely to be responsible for the variations in $\Delta^{56}Fe_{Fe(II)aq–Fe(III)am}$ fractionation. The molarity of Cl^- is 0.54 M in the experiments with AAS medium, as calculated using Geochemist's

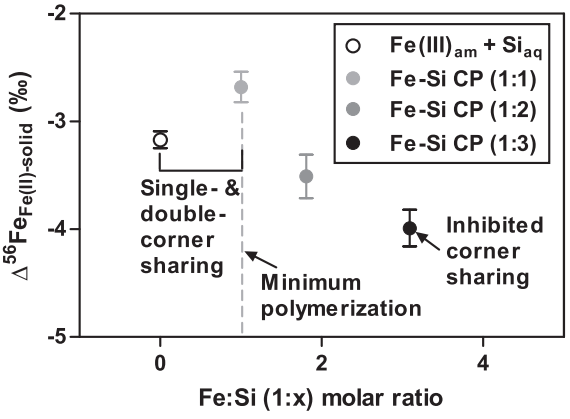

Fig. 6. Experimentally determined equilibrium isotope fractionation factor ($^{56}Fe/^{54}Fe$) between Fe(II) and pure $Fe(III)_{am}$ (in Si-containing solution) and Fe–Si CP (in Si-free solution) (Wu et al., 2011), and Fe–Si CP1 and Fe–Si CP2 in this study, versus the Fe:Si molar ratio of the solid. Structural characteristics that may affect isotopic fractionations noted for specific Fe:Si ratios.

Workbench (Bethke, 2002), which translates to a decrease of 0.16‰ for $\Delta^{56}Fe_{Fe(II)aq–Fe(III)am}$ when compared to experiments without AAS, assuming an average decrease of 0.3‰/M [Cl^-] in the fractionation factor (Hill et al., 2010). This value is within the error for the $\Delta^{56}Fe_{Fe(II)aq–Fe(III)am}$ fractionations (Table 1), and thus the impact from speciation changes can be considered negligible.

Because equilibrium stable isotope fractionations fundamentally reflect coordination environments (e.g., Schauble, 2004), the observed variation in $\Delta^{56}Fe_{Fe(II)aq–Fe(III)am}$ fractionation with Fe:Si ratio likely indicates alterations in the structure of the synthesized Fe–Si CP. As discussed below, these changes correspond with previously documented changes in local structure of Fe as a function of the Fe:Si of similar coprecipitates – specifically, changes in the proportions of different Fe octahedral linkages, such as single-, or double-corner sharing versus edge sharing.

Experimental studies using Fe K-edge EXAFS (Extended X-ray Absorption Fine Structure) spectroscopy have shown that Si ligands strongly influence the atomic environments of Fe during hydrolysis of Fe(III) (Doelsch et al., 2000). The Fe:Si ratios of the precipitates were determined to be very close to the initial ones used during hydrolysis (Doelsch et al., 2000), thus the structural properties determined in previous work are applicable to the precipitates used in the current study with the same Fe:Si ratios. The structural parameters for Fe in the first coordination sphere deduced from EXAFS analysis show that without Si, at pH 7, three atomic shells existed, consisting of Fe–O distances of 2.02, 1.89 and 2.18 Å. In contrast, at Fe:Si = 1:4, at pH 7, only two atomic shells occurred that had Fe–O distances of 2.00 and 1.85 Å. The lack of a third Fe–O atomic shell of longer Fe–O distance corresponds with the more negative $\Delta^{56}Fe_{Fe(II)aq–Fe(III)am}$ fractionations for Fe–Si CP1 (Fe:Si = 1:2) and CP2 (Fe:Si = 1:3) compared to $Fe(II)_{aq}$ and pure $Fe(III)_{am}$ (Fig. 6, Table 1). In addition, EXAFS analysis of the next-nearest coordination shells documented contributions from four Fe–Fe atomic shells: edge-sharing iron octahedra at approximately 3.00 and 3.10 Å, double-corner sharing iron octahedra at ~3.45 Å, and single-corner sharing iron octahedra at ~3.85 Å.

The Fe–O bond lengths together with the iron coordination determine how easy it would be to break the Fe–O bond, and in turn affect the equilibrium iron isotope fractionation factors. The relative contributions to Fe bonding from these different types of linkages change as a function of Si concentrations in the solid: when Fe:Si > 1, the growth

of $Fe(III)_{am}$ colloids is three dimensional, dominated by single- and double-corner sharing iron octahedra, whereas when Fe:Si < 1, Si ligands inhibit corner-sharing Fe octahedral linkages and promote a two-dimensional growth of Fe clusters through edge-sharing linkages. When Fe:Si = 1, Fe polymerization reaches a minimum, representing a crossover between the two growth regimes (Doelsch et al., 2000, 2003). Importantly, this change in local structure of Fe matches the inflection of our experimentally determined $\Delta^{56}Fe_{Fe(II)aq-Fe(III)am}$ fractionation (Fig. 6), i.e., the least negative fractionation factor for Fe–Si CP with Fe:Si = 1 corresponds to the minimum Fe polymerization, where the number of all types of linkages decreased and Fe growth sites were complexed by SiO_4 ligands. The increasingly negative fractionation factor determined for Fe–Si CP1 and CP2 can be attributed to an increase in the number of edge-sharing linkages and the decrease in the number of single- and double-corner sharing linkages at low Fe:Si ratio, as compared with no Si (Doelsch et al., 2003). In summary, Fe–Si polymerization exerts a significant effect on the equilibrium $Fe(II)_{aq}$–$Fe(III)_{am}$ fractionation factor, ~1.5‰ in $^{56}Fe/^{54}Fe$, over the range in Fe:Si ratios investigated. This is quite a large range for Fe isotopes, and this finding has important implications for interpreting Fe isotope data from natural Si-rich systems.

4.3. Isotopic exchange kinetics as controlled by movement of Fe(II) and Si

The combined results of this study and previous work (Wu et al., 2011), indicate that the kinetics of isotopic exchange between $Fe(II)_{aq}$ and different $Fe(III)_{am}$ phases is controlled by movement of Fe(II) and Si between aqueous and solid phases, rather than a simple bulk exchange mechanism. Isotopic exchange is initially rapid between $Fe(II)_{aq}$ and all $Fe(III)_{am}$ phases, as shown by the immediate increase in the fraction of isotope exchange after 30 min (Fig. 7). Because the pH of the point of zero charge (PZC) of $Fe(III)_{am}$ decreases from 8 to 4 in the presence of dissolved Si (Anderson and Benjamin, 1985), the Fe–Si CP in the current study was negatively charged at a pH of 6.7 and high adsorption of Fe(II) would be expected. The rapid initial isotope exchange can therefore be explained by net transfer of Fe(II) from aqueous to solid phase, promoting Fe isotope exchange between $Fe(II)_{aq}$ and the Fe–Si CP. This could ultimately be driven by the excess free energy of the surface defects in the initial solid.

The rates of isotopic exchange were controlled by Fe(II) and silica. High initial rates were associated with net loss of $Fe(II)_{aq}$ to the solid, and the slower rates of isotopic exchange at later time points may be explained by blockage of reactive surface sites by Si that was transferred from aqueous to solid phase (Fig. 3). We infer that adsorbed Si was strongly bound to surface Fe atoms in the Fe–Si CP, hindering further isotopic exchange after 2 days. Surface complexation modeling has shown that Si species bind directly to iron oxyhydroxide surfaces through inner-sphere complexes (Sigg and Stumm, 1981; Barrow and Bowden, 1987), which should inhibit atom exchange between Fe(II) and Fe(III) in the Fe–Si CP. Over long time periods, near-complete exchange was observed for $Fe(II)_{aq}$ and Fe–Si CP with 1:1 Fe:Si; in this case, Fe(II) moved from aqueous to solid phase as Si moved in the opposite direction (no aqueous Si in the beginning), which presumably freed reactive surface sites and promoted Fe(II) sorption and isotope exchange (Wu et al., 2011). This exchange is in agreement with ~80% isotopic exchange observed between Fe(II) and $Fe(III)_{am}$ in a previous study using a ^{55}Fe tracer (Pedersen et al., 2005), although it is important to note that phase transformations occurred in the ^{55}Fe

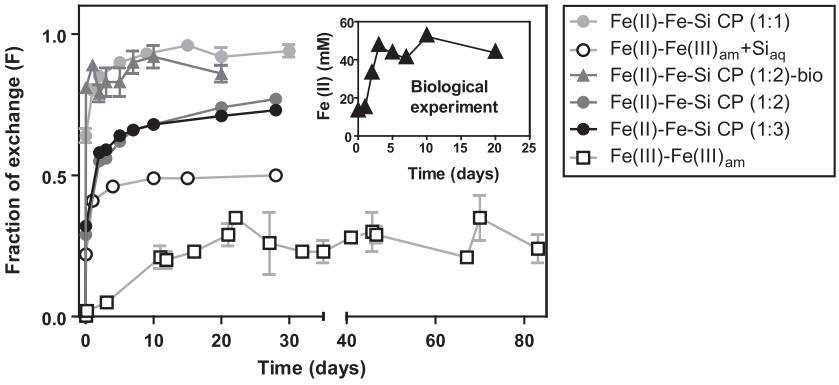

Fig. 7. Comparison of isotopic exchange kinetics for experiments with different $Fe(III)_{am}$ phases. The approximate Fe:Si ratio of Fe–Si coprecipitates is shown in parenthesis. Circles represent abiological experiments, and triangles represent results from the dissimilatory Fe(III) reduction experiments reported in Percak-Dennett et al. (2011). The inset shows the total Fe(II) produced with time in the 5 mM acetate experiments reported in Percak-Dennett et al. (2011). Data for pure $Fe(III)_{am}$ in Si-bearing solution ($Fe(III)_{am} + Si_{aq}$) and Fe–Si CP (1:1) are averages for four sets of experiments reported in Wu et al. (2011). Data for Fe–Si CP (1:2) and Fe–Si CP (1:3) are averages for duplicate reactors (Table EA5) in this study. The fraction of isotope exchange (F) for the biological experiment was calculated based on average $\Delta^{56}Fe_{Fe(II)aq-Fe(III)0.5M\ HCl}$ for each time point for the 5 mM acetate experiments reported in Percak-Dennett et al. (2011), divided by the fractionation factor determined for Fe(II)–Fe–Si CP (2:1) in this study (−3.51‰); as discussed in the text, we used data from the 5 mM acetate biological experiments for this comparison because these cultures had molar Fe(II)/Fe(III) ratios that overlaped the Fe(II)/Fe(III) ratios for the abiologic experiments in the current study. Data for exchange between Fe(III) and $Fe(III)_{am}$ is from Poulson et al. (2005).

tracer experiments and therefore these results also did not reflect true isotopic exchange reactions.

Isotopic exchange reached ~50% in the suspensions of pure $Fe(III)_{am}$ in Si-bearing solutions after 28 days (Fig. 7), where Si initially existed solely in the dissolved form. This result was unexpected, where it was anticipated that pure $Fe(III)_{am}$ would exchange more quickly than Fe–Si coprecipitates, based on the rapid reactions that occur in pure $Fe(II)_{aq}$–$Fe(III)_{am}$ systems (e.g., Pedersen et al., 2005). This result, however, demonstrates the key importance of Si in $Fe(II)_{aq}$–$Fe(III)_{am}$ systems. We attribute limited exchange that occurred in pure $Fe(III)_{am}$, Si-bearing solutions to reflect blockage of reactive surface sites by adsorbed Si, because Fe behaved conservatively with nearly constant molar proportion of each component with time (Wu et al., 2011). The rate and extent of exchange between $Fe(II)_{aq}$ and Fe–Si CP1 and Fe–Si CP2 (Fe–Si CP (1:2) and Fe–Si CP (1:3) in Fig. 7) was between that of the pure $Fe(III)_{am}$ (in Si containing solution) and Fe–Si CP (1:1, Si-free solution) systems examined in Wu et al. (2011) (Fig. 7), presumably reflecting a balance between (i) promotion of atom exchange by electron transfer, driven by the movement of Fe(II) from aqueous to the solid, and (ii) inhibition of atom exchange by blockage of surface sites through Si adsorption to solid surfaces.

4.4. Comparison of isotopic exchange kinetics between biological and abiological experiments

Our results on Fe isotope exchange during abiotic interaction of $Fe(II)_{aq}$ with Fe–Si CP may be compared to those of experiments on microbial reduction of analogous Fe–Si phases reported by Percak-Dennett et al. (2011). In the abiotic experiments (current study), a 1:1 molar ratio of aqueous Fe(II) to Fe(III) in the coprecipitate was used (2 mM $Fe(II)_{aq}$ plus 2 mM Fe–Si CP). In contrast, the DIR experiments produced a wide range of Fe(II):Fe(III) ratios as a result of progressive reduction of Fe(III) over time, and different amounts of electron donor (1–20 mM acetate) that were used to drive different overall degrees of Fe(III) reduction. The DIR experiments that employed 5 mM acetate produced Fe(II):Fe(III) ratios that are most directly comparable to the abiotic experiments of the current study, and the discussion below therefore focuses on that comparison.

The abiological experiments with Fe–Si CP1 conducted in this study employed exactly the same solid phase (~1:2 Fe:Si) and aqueous medium (Artificial Archean Seawater) used in the DIR experiments. A major, unavoidable difference, however, between the DIR and abiological experiments is that the entire quantity of $Fe(II)_{aq}$ was added to the start of the abiological experiments, whereas Fe(II) was produced over time in the microbial reduction experiments. Therefore, the redox driving force (e.g., high Fe(II)) for isotopic exchange was higher in the abiological experiments during the early time points, which would be expected to produce higher rates of initial exchange in the abiologic system. Contrary to this supposition, however, the fraction of isotopic exchange quickly reached ~70% after 30 min of initiating the DIR experiment (i.e., addition of the bacterial inoculum), in contrast to the ~30% exchange after the same time period in the abiological experiment of the current study (Fig. 7). The overall extent of isotopic exchange was also higher in the DIR experiments compared to that achieved during abiotic interaction between $Fe(II)_{aq}$ and Fe–Si CP1 (Fig. 7). The reason behind the faster initial exchange rate and higher long-term extent of exchange in the biological experiments remains unknown. One possible explanation is that the small amount of solid-phase Fe(II) introduced with the inoculum facilitated atom exchange in the beginning of the DIR experiments relative to the slower process of Fe(II) adsorption and incorporation of Fe(II) to Fe–Si CP1 in the abiological experiments. Such promotion of atom exchange by solid-phase Fe(II) may account for the near uniform fraction of exchange over time with increasing amounts of $Fe(III)_{am}$ reduction (Fig. 7).

There were significant differences in the nature of the Fe(II) components in the biological and abiological experiments. Percak-Dennett et al. (2011) proposed a structure for Fe–Si CP1, where an Fe(III)–Si–O network is formed by siloxane linkages between $Si(OH)_4$ molecules of a ferric silicate species. The large extent of reduction in the biological experiments must have greatly disrupted the original bonding arrangement between Fe(III) and Si. The majority of the Fe(II) produced throughout the course of DIR either adsorbed onto the solid surface or was incorporated into the interior of the solid, as indicated by HCl extraction assays. In contrast, Fe(II) moved slowly from aqueous to solid phase in the abiological experiments (Fig. 3), and the proportion of Fe(II) in the residual solid increased gradually with time, reaching only 17% of total Fe(II) after 28 days. The striking contrast between the biological and abiological systems thus apparently reflects the impact of enzymatic reduction versus simple mixing. These findings expand our understanding of the impact of DIR on aqueous/solid-phase Fe(II) partitioning and Fe isotope exchange. But, overall, comparison of "equivalent" abiologic and biologic $Fe(II)_{aq}$–$Fe(III)_{am}$ interactions suggest that biological systems may be more "reactive" in the sense of production of large quantities of Fe(II) that is accompanied by extensive isotopic exchange.

4.5. Implications for tracing biogeochemical cycling in the modern and ancient Earth

The equilibrium isotope fractionation factors and isotopic exchange kinetics determined in this study place fundamental constraints on the Fe isotope variations that would be expected in natural systems where aqueous Fe(II) and Fe–Si coprecipitates undergo isotopic exchange. The largest Fe isotope excursion in marine sedimentary rocks occurs between 2.7 and 2.4 Ga age, marked by $\delta^{56}Fe$ values as low as −4‰. Some workers have interpreted this to reflect microbial DIR (Johnson et al., 2008b). Others have argued that such negative $\delta^{56}Fe$ values reflect abiologic processes associated with redox changes, such as Fe(II) oxidation (e.g., Anbar and Rouxel, 2007), and still other studies have proposed that redox processes are not required and have favored partial utilization of aqueous Fe(II) during pyrite

formation as a mechanism for generation of low-δ^{56}Fe-bearing rocks (Guilbaud et al., 2011).

An important finding of the current study is the very large negative $\Delta^{56}Fe_{Fe(II)aq-Fe(III)am}$ fractionations measured for Fe–Si coprecipitates, as large as −4‰ for low Fe:Si ratios. Prior to this work, the maximum $^{56}Fe/^{54}Fe$ fractionation between Fe(III) and Fe(II) species was ~3‰. It is now recognized that Si-rich $Fe(III)_{am}$ phases were the most likely end products of Fe(II) oxidation and a likely precipitate in the photic zone of the Precambrian oceans (Konhauser et al., 2002; Kesler and Ohmoto, 2006). The relatively large negative $\Delta^{56}Fe_{Fe(II)aq-Fe(III)am}$ fractionations measured for Fe–Si coprecipitates may help explain the highly negative δ^{56}Fe values measured in some Precambrian marine sedimentary rocks, decreasing the need to call upon multiple redox cycling as an explanation for such low δ^{56}Fe values (Johnson and Beard, 2006; Wu et al., 2009). For example, a single step of 80% oxidation of $Fe(II)_{aq}$, occurring via biologically catalyzed processes in Precambrian oceans (Konhauser et al., 2002), or reaction with oxygen at circum-neutral pH (Millero et al., 1987), would produce δ^{56}Fe values of −3‰ for the remaining $Fe(II)_{aq}$ through oxidation under equilibrium conditions, or δ^{56}Fe values <−6‰ if a Rayleigh process was involved (Fig. 8). Large extents of oxidation of $Fe(II)_{aq}$ in the photic zone of an Archean ocean has been proposed as an explanation for the low δ^{56}Fe values that are found in Ca–Mg carbonates that contain low Fe contents, a carbonate composition that is commensurate with the small quantities of Fe(II) that are produced by oxidation (Czaja et al., 2010).

Oxidation of hydrothermally sourced $Fe(II)_{aq}$ in the photic zone of Archean or Proterozoic oceans would have produced a "rain" of $Fe(III)_{am}$–Si coprecipitates to the seafloor, and this mechanism is often cited for accumulation of Fe-rich deposits such as banded iron formations (BIFs) (e.g., Klein, 2005; Beukes and Gutzmer, 2008). The near-zero average δ^{56}Fe value for the very large 2.5 Ga BIFs from South Africa and Australia suggests that the average δ^{56}Fe value of the Fe–Si coprecipitate "rain" was near zero for these rocks (Johnson et al., 2003, 2008a), and yet on a fine scale (dm to mm), the δ^{56}Fe values of these BIFs vary greatly (e.g., Johnson et al., 2003, 2008a; Heimann et al., 2010; Craddock and Dauphas, 2011). Given the results of the present study, could this range in δ^{56}Fe values record abiologic isotopic exchange between pore fluid $Fe(II)_{aq}$ and Fe–Si coprecipitates, or is a role for biology required? We address this question below by considering the depositional and diagenetic environments of BIF formation, with a focus on the proportions of aqueous Fe(II) and Fe–Si coprecipitates, in recognition that both phases are required to induce isotopic exchange.

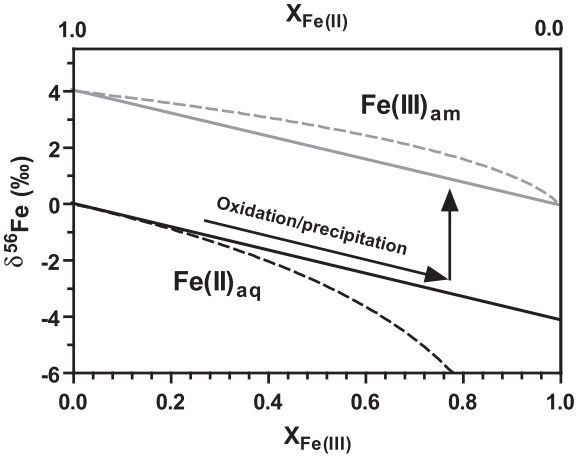

Fig. 8. Isotopic relations produced by extensive oxidation and precipitation of $Fe(II)_{aq}$. Solid lines indicate maximum equilibrium fractionation factor between $Fe(II)_{aq}$ and $Fe(III)_{am}$; as obtained in this study, and dashed lines indicate a Rayleigh fractionation that has the same fractionation factor.

Fe–Si coprecipitates that were deposited on the seafloor early in BIF deposition likely underwent dehydration and conversion to hematite and chert (e.g., Klein and Bricker, 1977; Ewers and Morris, 1981). Hematite is rare in BIFs that have not been subjected to post-depositional ore-forming processes, but hematite that may be related to "primary" Fe–Si coprecipitates is found in chert and siderite/ankerite layers in the extensive 2.5 Ga BIFs from South Africa and Australia (e.g., Beukes et al., 1990; Johnson et al., 2003; Beukes and Gutzmer, 2008, 2008a; Heimann et al., 2010). Prior to conversion to hematite, equilibrium isotopic exchange between pore fluid $Fe(II)_{aq}$ and Fe–Si coprecipitates would produce solids with high δ^{56}Fe values if high proportions of $Fe(II)_{aq}$ vs. low proportions of Fe–Si coprecipitates are assumed, or near-zero δ^{56}Fe values if low proportions of $Fe(II)_{aq}$ vs. high proportions of Fe–Si coprecipitates are assumed (Fig. 8). That the bulk δ^{56}Fe values of 2.5 Ga BIFs lie near zero suggests that only small quantities of $Fe(II)_{aq}$ were included in pore fluids during primary BIF deposition. This is supported by the observation that many occurrences of the "primary" hematite that is found in the large 2.5 Ga BIFs is included in chert bands that contain few other Fe minerals (Beukes et al., 1990; Johnson et al., 2003; Beukes and Gutzmer, 2008). We conclude that in the case of accumulation of Fe–Si coprecipitates and only small quantities of pore fluid $Fe(II)_{aq}$, there would be little driving force for the extensive fluid–solid isotopic exchange that would be required to produce the wide range of δ^{56}Fe values observed in BIFs. Given the high Fe(II) sorption capacity of the Fe–Si coprecipitates studied here, significant quantities of seawater $Fe(II)_{aq}$ would need to be buried (i.e., by burial advection) with BIF sediment to retain significant quantities of $Fe(II)_{aq}$. The molar Fe mass balance in the sediment and pore fluid is critical, therefore, because pore fluid is the only mobile Fe-bearing phase that could effectively propagate isotopic heterogeneity through the BIF sediment column.

Hematite that reflects "primary" iron oxyhydroxides is also found as inclusions in siderite/ankerite layers in BIFs (Beukes et al., 1990; Beukes and Gutzmer, 2008), and such a relation might be interpreted to indicate burial of Fe–Si coprecipitates with large quantities of pore fluid $Fe(II)_{aq}$. New studies, however, demonstrate that the majority of siderite and ankerite in the 2.5 Ga BIFs have C, O, Fe, and Sr isotope compositions that rule out precipitation from seawater or from pore fluids of seawater derivation (Heimann

et al., 2010; Ludois, 2010; Craddock and Dauphas, 2011). This in turn suggests that the Fe(II) inventory in siderite/ankerite layers in at least the 2.5 Ga South African and Australian BIFs that have been studied to date must have had an origin other that entrapment of seawater $Fe(II)_{aq}$ during burial.

In situ generation of pore fluid $Fe(II)_{aq}$ by microbial DIR seems the most likely explanation for producing the significant quantities of $Fe(II)_{aq}$ that are required to catalyze isotopic exchange with Fe–Si coprecipitates, followed by migration through the BIF sediment. Delivery of Fe–Si hydroxides from the photic zone, in addition to organic carbon produced by photosynthesis in the shallow ocean, would provide the "fuel" required to sustain active DIR in non-lithified BIF sediment (e.g., Walker, 1984; Konhauser et al., 2005). In this model, isotopic exchange of $Fe(II)_{aq}$ and Fe–Si coprecipitates may occur without a direct role for biology, although we note that the current study demonstrated higher rates of exchange for biologic systems relative to abiologic experiments that used the same Fe–Si coprecipitate. Instead, the role for biology probably lies in providing the sizeable $Fe(II)_{aq}$ inventory that is required to catalyze isotopic exchange and distribute a range of isotopic compositions throughout the sediment. Given the arguments above, *in situ* production of $Fe(II)_{aq}$ by DIR that is supplied by Fe–Si coprecipitates and organic carbon "rain" from the photic zone would seem to be a far more likely explanation for the Fe isotope heterogeneities observed in BIFs than simple isotopic exchange between Fe–Si coprecipitates and the limited quantities of seawater $Fe(II)_{aq}$ that would be sequestered in the sediment.

We next turn to Fe isotope variations in Fe-rich rocks such as organic carbon-rich shales. Several studies have argued that net Fe enrichment is well explained by a "basin Fe shuttle" (Raiswell and Anderson, 2005; e.g., Lyons and Severmann, 2006), and this concept has been extended to Fe isotopes (Severmann et al., 2008), where negative δ^{56}Fe values for Fe-rich samples has been interpreted to reflect DIR. Severmann et al. (2008) noted that the apparent fractionation between $Fe(II)_{aq}$ and amorphous iron oxides, in experiment or modern marine environments (e.g., Severmann et al., 2006; Rouxel et al., 2008) is insufficient to explain the highly negative δ^{56}Fe values measured in many Neoarchean and Paleoproterozoic black shales, and they additionally called upon a fractionation between $Fe(II)_{aq}$ and pyrite. If, however, the much larger isotopic fractionations measured here between $Fe(II)_{aq}$ and Fe–Si coprecipitate were applicable, as seems likely in the Precambrian, the Fe isotope fractionations produced by a DIR-driven basin shuttle would be more extreme than those inferred based on modern marine systems.

It has been recently proposed that abiological precipitation of pyrite may produce the negative δ^{56}Fe values seen in the Late Archean and Early Proterozoic rock record, which contrasts with the redox-driven models discussed above (Guilbaud et al., 2011). Guilbaud et al. (2011) interpret the kinetic isotope fractionations associated with FeS and pyrite formation measured in their laboratory experiments to be a viable mechanism for producing δ^{56}Fe values as low as $-4‰$. This model requires that the highly negative δ^{56}Fe values be restricted to an inventory that represents only a few percent of the initial $Fe(II)_{aq}$ inventory. The model of Guilbaud et al. (2011), therefore, might be an explanation for small quantities of individual low-δ^{56}Fe pyrite grains in shales, but it cannot explain the presence of Fe-rich rocks that have low δ^{56}Fe values (Czaja et al., 2012). Moreover, the Guilbaud et al. (2011) model cannot explain the range in δ^{56}Fe values for BIFs, which contain very low sulfide contents (e.g., Klein, 2005).

We conclude that the equilibrium Fe isotope fractionations factors and kinetics of isotopic exchange determined here, and in previous studies, provide the fundamental information needed to interpret Fe isotope fractionation pathways in modern and ancient natural systems. However, full understanding of these pathways requires assessment of depositional and diagenetic processes and consideration of Fe mass balance to understand what rocks will record evidence for which process. There is as yet no proven "vital" effect for Fe isotope fractionation that is uniquely biological. It would be short-sighted, however, to conclude that the lack of a "vital" effect decreases the need to call upon biological cycling of Fe. The key issue in explaining the range of Fe isotope compositions in the ancient rock record is interaction of significant quantities of mobile, aqueous Fe(II) with Fe(III) oxyhydroxides such that isotopic exchange will occur. We argue that in a number of settings, such as the environments of BIF deposition, DIR is the most likely means of providing large quantities of $Fe(II)_{aq}$ via *in situ* reduction in the sediment section prior to lithification.

5. CONCLUSIONS

This study determined the equilibrium isotope fractionation factors between $Fe(II)_{aq}$ and amorphous Fe(III) oxide–Si coprecipitates under conditions that simulated Archean seawater conditions. Using the three-isotope method, $^{56}Fe/^{54}Fe$ fractionation factors of $-3.51 \pm 0.20‰$ and $-3.99 \pm 0.17‰$ were determined for isotope exchange between $Fe(II)_{aq}$ and Fe–Si coprecipitates with Fe:Si ratios of 1:2 and 1:3, respectively. The equilibrium fractionation factor between $Fe(II)_{aq}$ and $Fe(III)_{am}$ changed as a function of the Fe:Si molar ratio of the solid, where the fractionation is least negative when Fe:Si = 1:1, and the most negative when Fe:Si = 1:3. This corresponds with changes in the local structure of Fe in the Fe–Si coprecipitates, as determined using spectroscopic methods (Doelsch et al., 2003). These findings demonstrate that stable isotope fractionation reflects the local structure of different Fe(III) oxyhydroxides including poorly crystalline, amorphous materials. Moreover, these results show that the fractionation factor may be significantly larger than previously thought as compared to experimental results obtained on simple systems, or inferred from modern environments where dissolved silica is not present.

Comparison of Fe isotope exchange between Fe(II) and different $Fe(III)_{am}$ phases showed that movement of Fe(II) and Si controlled the kinetics of isotopic exchange. Near complete isotope exchange occurred in systems that initially contained Fe–Si coprecipitates in the absence of aqueous Si, where Fe(II) moved from aqueous to solid in opposition to

the direction of Si partitioning. In contrast, only ~50% exchange was achieved in systems that contained pure amorphous Fe(III) oxide with 2.1 mM aqueous Si in solution, likely reflecting blockage of reactive surface sites by sorbed Si. Approximately 75% exchange was reached in systems that contained Fe–Si coprecipitates with 2.1 mM Si in solution, in which both Fe(II) and Si were partitioned into the solid-phase over time. The much higher extent of isotopic exchange between $Fe(II)_{aq}$ and Fe(III) oxyhydroxides compared with that between aqueous Fe(III) and ferrihydrite clearly demonstrates the importance of electron exchange in promoting iron atom exchange. The isotopic exchange kinetics determined here indicate that isotopic exchange in natural systems, particularly in the presence of dissolved silica, likely requires significant quantities of pore fluid $Fe(II)_{aq}$.

These findings provide constraints for equilibrium fractionation factors between $Fe(II)_{aq}$ and $Fe(III)_{am}$ produced by different geochemical processes, which can in turn serve as a framework for interpreting iron isotope data in natural environments that contain reduced and oxidized iron. Moreover, comparison of abiological and biological experiments demonstrates that coupled electron and atom exchange between Fe(II) and Fe(III) oxyhydroxide is likely to be a universal mechanism for Fe isotope fractionation in natural systems that contain reduced and oxidized Fe. Systems that undergo large extents of oxidation, such as in the photic zone of Archean oceans, are expected to produce only a small amount of $Fe(II)_{aq}$ that has low-δ^{56}Fe values. In contrast, *in situ* partial microbial Fe(III) reduction in the environments that formed banded iron formations (BIFs) likely represents the most effective means for juxtaposition of significant quantities of pore fluid $Fe(II)_{aq}$ and Fe–Si coprecipitates. Separation in space and time of isotopically light Fe(II) from residual heavy Fe(III) would in turn produce the fine-scale Fe isotope heterogeneities found in BIFs.

ACKNOWLEDGEMENTS

This research was supported by the NASA Astrobiology Institute. We thank Hiromi Konishi for TEM work and Huifang Xu for discussion on the local structure of Fe–Si coprecipitates.

APPENDIX A. SUPPLEMENTARY DATA

Supplementary data associated with this article can be found, in the online version, at doi:10.1016/j.gca.2012.01.007.

REFERENCES

Anbar A. D. and Rouxel O. (2007) Metal stable isotopes in paleoceanography. *Annu. Rev. Earth Planet. Sci.* **35**, 717–746.

Anderson P. R. and Benjamin M. M. (1985) Effect of silicon on the crystallization and adsorption properties of ferric oxides. *Environ. Sci. Technol.* **19**, 1048–1053.

Barrow N. J. and Bowden J. W. (1987) A comparison of models for describing the adsorption of anions A on a variable charge mineral surface. *J. Colloid Interf. Sci.* **119**, 236–250.

Beard B. L., Handler R. M., Scherer M. M., Wu L., Czaja A. D., Heimann A. and Johnson C. M. (2010) Iron isotope fractionation between aqueous ferrous iron and goethite. *Earth Planet. Sci. Lett.* **295**, 241–250.

Beard B. L., Johnson C. M., Skulan J. L., Nealson K. H., Cox L. and Sun H. (2003) Application of Fe isotopes to tracing the geochemical and biological cycling of Fe. *Chem. Geol.* **195**, 87–117.

Bergquist B. A. and Boyle E. A. (2006) Iron isotopes in the Amazon River system: weathering and transport signatures. *Earth Planet. Sci. Lett.* **248**, 54–68.

Bethke C. M. (2002) The Geochemist's Workbench 4.0. Urbana, IL.

Beukes N. J. and Gutzmer J. (2008) Origin and paleoenvironmental significance of major iron formations at the Archean–Paleoproterozoic boundary. *Soc. Eco. Geo. Rev.* **15**, 5–47.

Beukes N. J., Klein C., Kaufman A. J. and Hayes J. M. (1990) Carbonate petrography, kerogen distribution, and carbon and oxygen isotope variations in an Early Proterozoic transition from limestone to iron-formation deposition, Transvaal Supergroup, South Africa. *Econ. Geol.* **85**, 663–690.

Clesceri L. S., Greenberg A. E. and Eaton A. D. (1989) *Standard Methods for the Examination of Water and Wastewater*. American Public Health Association, Washington, DC.

Cornell R. M. and Schwertmann U. (2003) The iron oxides: Structure, Properties, Reactions, Occurrences, and Uses. Wiley-VCH, Weinheim.

Craddock P. R. and Dauphas N. (2011) Iron and carbon isotope evidence for microbial iron respiration throughout the Archean. *Earth Planet. Sci. Lett.* **303**, 121–132.

Crosby H. A., Johnson C. M., Roden E. E. and Beard B. L. (2005) Coupled Fe(II)–Fe(III) electron and atom exchange as a mechanism for Fe isotope fractionation during dissimilatory iron oxide reduction. *Environ. Sci. Technol.* **39**, 6698–6704.

Crosby H. A., Roden E. E., Johnson C. M. and Beard B. L. (2007) The mechanisms of iron isotope fractionation produced during dissimilatory Fe(III) reduction by *Shewanella putrefaciens* and *Geobacter sulfurreducens*. *Geobiology*. doi:10.1111/j.1472-4669.2007.00103.x.

Czaja A. D., Johnson C. M., Yamaguchi K. E. and Beard B. L. (2012) Comment on "Abiotic Pyrite Formation Produces a Large Fe Isotope Fractionation". *Science* **335**, 538.

Czaja A. D., Johnson C. M., Beard B. L., Eigenbrode J. L., Freeman K. H. and Yamaguchi K. E. (2010) Iron and carbon isotope evidence for ecosystem and environmental diversity in the ~2.7 to 2.5 Ga Hamersley Province, Western Australia. *Earth Planet. Sci. Lett.* **292**, 170–180.

Doelsch E., Masion A., Rose J., Stone W. E. E., Bottero J. Y. and Bertsch P. M. (2003) Chemistry and structure of colloids obtained by hydrolysis of Fe(III) in the presence of SiO_4 ligands. *Colloid Surf. A* **217**, 121–128.

Doelsch E., Rose J., Masion A., Bottero J. Y., Nahon D. and Bertsch P. M. (000) Speciation and crystal chemistry of iron(III) chloride hydrolyzed in the presence of SiO_4 ligands. 1, An Fe K-edge EXAFS study. *Langmuir* **16**, 4726–4731.

Doelsch E., Stone W. E. E., Petit S., Masion A., Rose J., Bottero J. Y. and Nahon D. (2001) Speciation and crystal chemistry of Fe(III) chloride hydrolyzed in the presence of SiO_4 ligands. 2. Characterization of Si–Fe aggregates by FTIR and ^{29}Si solid-state NMR. *Langmuir* **17**, 1399–1405.

Ewers W. E. and Morris R. C. (1981) Studies of the Dales Gorge member of the Brockman Iron Formation, Western Australia. *Econ. Geol.* **76**, 1929–1953.

Fehr M. A., Andersson P. S., Hålenius U. and Mörth C.-M. (2008) Iron isotope variations in Holocene sediments of the Gotland Deep, Baltic Sea. *Geochim. Cosmochim. Acta* **72**, 807–826.

Guilbaud R., Butler I. B. and Ellam R. M. (2011) Abiotic pyrite formation produces a large Fe isotope fractionation. *Science* **332**, 1548–1551.

Habicht K., Gade M., Thamdrup B., Berg P. and Canfield D. (2002) Calibration of sulfate levels in the Archean Ocean. *Science* **298**, 2372–2374.

Heimann A., Johnson C. M., Beard B. L., Valley J. W., Roden E. E., Spicuzza M. J. and Beukes N. J. (2010) Fe, C, and O isotope compositions of banded iron formation carbonates demonstrate a major role for dissimilatory iron reduction in ~2.5 Ga marine environments. *Earth Planet. Sci. Lett.* **294**, 8–18.

Hill P. S., Schauble E. A. and Young E. D. (2010) Effects of changing solution chemistry on Fe^{3+}/Fe^{2+} isotope fractionation in aqueous Fe–Cl solutions. *Geochim. Cosmochim. Acta* **74**, 6669–6689.

Icopini G. A., Anbar A. D., Ruebush S. S., Tien M. and Brantley S. L. (2004) Iron isotope fractionation during microbial reduction of iron: the importance of adsorption. *Geology* **32**, 205–208.

Johnson C. and Beard B. (2006) Fe isotopes: an emerging technique in understanding modern and ancient biogeochemical cycles. *GSA Today* **16**, 4–10.

Johnson C., Roden E., Welch S. and Beard B. (2005) Experimental constraints on Fe isotope fractionation during magnetite and Fe carbonate formation coupled to dissimilatory hydrous ferric oxide reduction. *Geochim. Cosmochim. Acta* **69**, 963–993.

Johnson C. M., Beard B. L., Beukes N. J., Klein C. and O'Leary J. M. (2003) Ancient geochemical cycling in the Earth as inferred from Fe isotope studies of banded iron formations from the Transvaal Craton. *Contrib. Mineral. Petrol.* **144**, 523–547.

Johnson C. M., Beard B. L., Klein C., Beukes N. J. and Roden E. E. (2008a) Iron isotopes constrain biologic and abiologic processes in banded iron formation genesis. *Geochim. Cosmochim. Acta* **72**, 151–169.

Johnson C. M., Beard B. L. and Roden E. E. (2008b) The iron isotope fingerprints of redox and biogeochemical cycling in modern and ancient Earth. *Annu. Rev. Earth Planet. Sci.* **36**, 457–493.

Johnson C. M., Skulan J. L., Beard B. L., Sun H., Nealson K. H. and Braterman P. S. (2002) Isotopic fractionation between Fe(III) and Fe(II) in aqueous solutions. *Earth Planet. Sci. Lett.* **195**, 141–153.

Kesler S. E. and Ohmoto H. (2006) *Evolution of early earth's atmosphere, hydrosphere, and biosphere: constraints from ore deposits*. Geological Society of America, Boulder, Colo.

Kester D., Duedall I., Connors D. and Pytkowic R. M. (1967) Preparation of artificial seawater. *Limnol. Oceanogr.* **12**, 176–179.

Klein C. (2005) Some Precambrian banded iron-formations (BIFs) from around the world: their age, geologic setting, mineralogy, metamorphism, geochemistry, and origins. *Am. Mineral.* **90**, 1473–1499.

Klein C. and Bricker O. P. (1977) Some aspects of the sedimentary and diagenetic environment of Proterozoic banded iron-formation. *Econ. Geol.* **72**, 1457–1470.

Konhauser K., Hamade T., Raiswell R., Morris R., Ferris F., Southam G. and Canfield D. (2002) Could bacteria have formed the Precambrian banded iron formations? *Geol* **30**, 1079–1082.

Konhauser K., Newman D. and Kappler A. (2005) The potential significance of microbial Fe (III) reduction during deposition of Precambrian banded iron formations. *Geobiology* **3**, 167–177.

Konhauser K. O., Lalonde S. V., Amskold L. and Holland H. D. (2007) Was there really an Archean phosphate crisis? *Science* **315**, 1234.

Krishnamurti G. S. R. and Huang P. M. (1990) Spectrophometric determination of Fe(II) with 2, 4, 6-Tri(2′-pyridyl)-1,3, 5-Triazine in the presence of large quantities of Fe(III) and complexing ions. *Talanta* **37**, 745–748.

Li W., Beard B. L. and Johnson C. M. (2011) Exchange and fractionation of Mg isotopes between epsomite and saturated MgSO4 solution. *Geochim. Cosmochim. Acta* **75**, 1814–1828.

Ludois J. M. (2010) Strontium isotopes in banded iron formation carbonates: disequilibrium with ancient seawater. Master thesis, University of Wisconsin-Madison.

Lyons T. W. and Severmann S. (2006) A critical look at iron paleoredox proxies: new insights from modern euxinic marine basins. *Geochim. Cosmochim. Acta* **70**, 5698–5722.

Maliva R. G., Knoll A. H. and Simonson B. M. (2005) Secular change in the Precambrian silica cycle: insights from chert petrology. *Geol. Soc. Am. Bull.* **117**, 835–845.

Matsuhisa Y., Goldsmith J. R. and Clayton R. N. (1978) Mechanisms of hydrothermal crystallization of quartz at 250 °C and 15 kbar. *Geochim. Cosmochim. Acta* **42**, 173–182.

Millero F. J., Sotolongo S. and Izaguirre M. (1987) The oxidation kinetics of Fe(II) in seawater. *Geochim. Cosmochim. Acta* **51**, 793–801.

Pedersen H. D., Postma D., Jakobsen R. and Larsen O. (2005) Fast transformation of iron oxyhydroxides by the catalytic action of aqueous Fe(II). *Geochim. Cosmochim. Acta* **69**, 3967–3977.

Percak-Dennett E. M., Roden E. E., Beard B. L. and Johnson C. M. (2011) Iron isotope fractionation during dissimilatory iron reduction under simulated Archean conditions. *Geobiology* **9**, 205–220.

Poulson R. L., Johnson C. M. and Beard B. L. (2005) Iron isotope exchange kinetics at the nanoparticulate ferrihydrite surface. *Am. Mineral.* **90**, 758–763.

Raiswell R. and Anderson T. F. (2005) Reactive iron enrichment in sediments deposited beneath euxinic bottom waters: constraints on supply by shelf recycling. In *Mineral Deposits and Earth Evolution Geological Society, London, Special Publication 248* (eds. I. McDonald, A. J. Boyce, I. B. Butler, R. J. Herrington and D. A. Polya). Geological Society, London.

Rouxel O., Sholkovitz E., Charette M. and Edwards K. J. (2008) Iron isotope fractionation in subterranean estuaries. *Geochim. Cosmochim. Acta* **72**, 3413–3430.

Schauble E. A. (2004) Applying stable isotope fractionation theory to new systems. *Rev. Mineral. Geochem.* **55**, 65–111.

Severmann S., Johnson C. M., Beard B. L. and McManus J. (2006) The effect of early diagenesis on the Fe isotope compositions of porewaters and authigenic minerals in continental margin sediments. *Geochim. Cosmochim. Acta* **70**, 2006–2022.

Severmann S., Lyons T. w., Anbar A., McManus J. and Gordon G. (2008) Modern iron isotope perspective on the benthic iron shuttle and the redox evolution of ancient oceans. *Geology* **36**, 487–490.

Severmann S., McManus J., Berelson W. M. and Hammond D. E. (2010) The continental shelf benthic iron flux and its isotope composition. *Geochim. Cosmochim. Acta* **74**, 3984–4004.

Shahar A., Young E. D. and Manning C. E. (2008) Equilibrium high-temperature Fe isotope fractionation between fayalite and magnetite: an experimental calibration. *Earth Planet. Sci. Lett.* **268**, 330–338.

Sigg L. and Stumm W. (1981) The interaction of anions and weak acids with the hydrous goethite (α-FeOOH) surface. *Colloids Surf.* **2**, 101–117.

Staubwasser M., von Blanckenburg F. and Schoenberg R. (2006) Iron isotopes in the early marine diagenetic iron cycle. *Geology* **34**, 629–632.

Stoffregen R. E., Rye R. O. and Wasserman M. D. (1994) Experimental studies of alunite: II. Rates of alunite–water alkali and isotope exchange. *Geochim. Cosmochim. Acta* **58**, 917–929.

Stookey L. (1970) Ferrozine: a new spectrophotometric reagent for iron. *Anal. Chem.* **42**, 779–781.

Tangalos G. E., Beard B. L., Johnson C. M., Alpers C. N., Shelobolina E. S., Xu H., Konishi H. and Roden E. E. (2010) Microbial production of isotopically light iron(II) in a modern chemically precipitated sediment and implications for isotopic variations in ancient rocks. *Geobiology* **8**, 197–208.

Teutsch N., Schmid M., Muller B., Halliday A. N., Burgmann H. and Wehrli B. (2009) Large iron isotope fractionation at the oxic-anoxic boundary in Lake Nyos. *Earth Planet. Sci. Lett.* **285**, 52–60.

Walker J. (1984) Suboxic diagenesis in Banded Iron Formaitons. *Nature* **309**, 340–342.

Welch S. A., Beard B. L., Johnson C. M. and Braterman P. S. (2003) Kinetic and equilibrium Fe isotope fractionation between aqueous Fe(II) and Fe(III). *Geochim. Cosmochim. Acta* **67**, 4231–4250.

Williams A. G. B. and Scherer M. M. (2004) Spectroscopic evidence for Fe(II)–Fe(III) electron transfer at the iron oxide–water interface. *Environ. Sci. Technol.* **38**, 4782–4790.

Wu L., Beard B. L., Roden E. E. and Johnson C. M. (2009) Influence of pH and dissolved Si on Fe isotope fractionation during dissimilatory microbial reduction of hematite. *Geochim. Cosmochim. Acta* **73**, 5584–5599.

Wu L., Beard B. L., Roden E. E. and Johnson C. M. (2011) Stable iron isotope fractionation between aqueous Fe(II) and hydrous ferric oxide. *Environ. Sci. Technol.* **45**, 1847–1852.

Wu L., Beard B. L., Roden E. E., Kennedy C. B. and Johnson C. M. (2010) Stable Fe isotope fractionation produced by aqueous Fe(II)–hematite surface interactions. *Geochim. Cosmochim. Acta* **74**, 4249–4265.

Zink S., Schoenberg R. and Staubwasser M. (2010) Isotopic fractionation and reaction kinetics between Cr(III) and Cr(VI) in aqueous media. *Geochim. Cosmochim. Acta* **74**, 5729–5745.

Associate editor: Derek Vance